CrossMark

RESEARCH PAPER

Numerical simulation of GMAW process using Ar and an Ar–CO$_2$ gas mixture

Yosuke Ogino[1] · Yoshinori Hirata[1] · Anthony B. Murphy[2]

Abstract The gas metal arc welding (GMAW) process involves arc plasma, metal transfer, and weld pool phenomena. In addition, metal vapor is formed by evaporation from the high-temperature metal and mixes with the arc plasma. These phenomena interact with each other and are very complicated. A numerical approach that includes their interaction is therefore important for clarifying the GMAW phenomena. We have developed a unified model and used the model to investigate the influence of the shielding gas on the metal transfer. When argon shielding gas was used, for an arc current of less than 230 A, globular transfer occurred. For higher currents, spray transfer occurred. On the other hand, when Ar + 18 %CO$_2$ gas was used, the transition from globular to spray transfer occurred at around 280 A. This difference was caused by changes in the driving force exerted on the molten metal by the arc plasma. The arc pressure that lifts up the molten metal and interferes with its detachment from the wire tip becomes stronger when the gas mixture is used.

Recommended for publication by Study Group 212 - The Physics of Welding

✉ Yosuke Ogino
   ogino@mapse.eng.osaka-u.ac.jp

1   Graduate School of Engineering, Osaka University, Suita, Japan

2   CSIRO Manufacturing, Lindfield, Australia

1 Introduction

Gas metal arc welding (GMAW) is a highly productive process that is an indispensable technology in many industrial fields. It uses consumable wire electrodes, with molten metal detaching from the wire tip and transferring through the arc to the base metal. The properties of the metal transfer, such as the droplet size and frequency of transfer, strongly affect the stability and quality of the overall process. Therefore, appropriate control of the metal transfer is highly desirable. However, there are many different transfer modes [1], and the process is not yet fully understood due to its complexity, so it is difficult to control the metal transfer completely. Free-flight transfer, for example, can be divided into globular transfer and spray transfer. Globular transfer occurs at low currents. In this mode, a large droplet forms at the wire tip and falls to the base metal under the influence of gravity. On the other hand, spray transfer occurs at relatively high currents. Many small droplets are sprayed onto the base metal in this mode. Spray transfer is desirable in industrial fields because of its high stability and low spatter generation.

In order to understand the metal transfer phenomena, considerable research has been performed [2–4]. The transfer mode changes depending on welding conditions such as the arc current, welding voltage, and electrode radius [5]. The shielding gas also affects the transfer mode. When an Ar–CO$_2$ gas mixture is used, a higher arc current is necessary to obtain spray transfer than when pure Ar is used. Moreover, when CO$_2$ or He is used, spray transfer does not occur even for high arc currents [6].

Many investigations based on numerical simulations have also been performed. Recently, with the dramatic improvement in computing technology, many dynamic models based on computational fluid dynamics (CFD) have been reported [7–12]. In particular, a unified model that includes interactions

between the arc plasma and the metal transfer is a very powerful tool for understanding the metal transfer phenomena [13–17]. However, there are few reports that discuss the influence of the shielding gas. For example, Haidar et al. reported the influence of CO_2 gas on droplet formation by using numerical model, but their model does not consider the influence of metal vapor [18].

The objective of this research is to understand the metal transfer phenomena more deeply with a strong focus on the influence of the shielding gas on the metal transfer. We numerically investigate the influence of the arc current on the metal transfer using Ar and an Ar–CO_2 gas mixture as the shielding gas. In addition, the mechanism responsible for the difference in the transfer mode is discussed.

2 Simulation model

A simulation model that includes the interactions between the arc plasma, the metal transfer, and the weld pool is constructed in this study. However, it is difficult to calculate these phenomena simultaneously because of the difference in the material properties and velocity scales. For this reason, the arc plasma and the molten metal were treated as two separate fluids in the model. At one time step, the characteristics of the arc plasma (such as the temperature, velocity, and pressure fields) are calculated first for a fixed molten metal shape. Then, the characteristics of the molten metal are calculated using the arc plasma characteristics as the boundary conditions. At the next time step, the arc plasma is calculated using the new molten metal shape as the boundary condition. These calculations are performed repeatedly, allowing the development of both the droplet and the arc plasma over time to be calculated, as shown in Fig. 1.

The following method was used to calculate the arc plasma phenomena. Under the local thermodynamic equilibrium (LTE) approximation, the arc plasma can be treated as a viscous electromagnetic fluid. Therefore, the thermal and electromagnetic fluid phenomena are governed by the following equations:
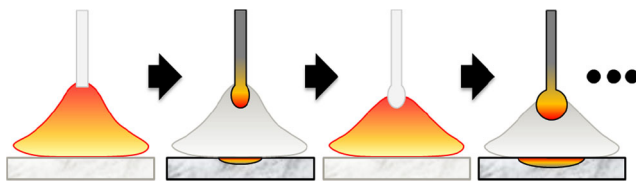
$$\nabla \cdot \left(\rho \overrightarrow{v} \right) = S, \tag{1}$$

Fig. 1 Schematic explanation of calculation procedure for this model

$$\frac{\partial \left(\rho \overrightarrow{v} \right)}{\partial t} + \nabla \cdot \left(\rho \overrightarrow{v} \, \overrightarrow{v} \right) = -\nabla P + \nabla \cdot \boldsymbol{\tau} + \rho \overrightarrow{g} + \overrightarrow{F}_{em}, \tag{2}$$

$$\frac{\partial (\rho H)}{\partial t} + \nabla \cdot \rho \overrightarrow{v} H = -\nabla \cdot (-\kappa \nabla T) + W - Ra + S_E, \tag{3}$$

where $\overrightarrow{v}$ is the velocity [m/s], t is the time [s], ρ is the density [kg/m³], P is the pressure [Pa], $\boldsymbol{\tau}$ is the viscous stress tensor [Pa], $\overrightarrow{g}$ is the gravitational acceleration [m/s²], H is the enthalpy [J/kg], κ is the thermal conductivity [W/m/K], T is the temperature [K], Ra is the radiative loss [W/m³], $\overrightarrow{F}_{em}$ is the electromagnetic force [N/m³], W is the Joule heating [W/m³], S is the source term of metal vapor mass [kg/m³/s], and S_E is the source term of metal vapor energy [W/m³]. The electromagnetic force and the Joule heating can be calculated using the following equations:

$$\overrightarrow{F}_{em} = \overrightarrow{j} \times \overrightarrow{B}, \tag{4}$$

$$W = \frac{\left| \overrightarrow{j} \right|^2}{\sigma}, \tag{5}$$

where $\overrightarrow{j}$ is the current density [A/m²], $\overrightarrow{B}$ is the magnetic flux density [T], and σ is the electrical conductivity [S/m]. The current density and the magnetic flux density can be calculated by the following equations:

$$\nabla \cdot \overrightarrow{j} = 0, \tag{6}$$

$$\overrightarrow{j} = -\sigma \nabla V, \tag{7}$$

$$\overrightarrow{B} = \nabla \times \overrightarrow{A}, \tag{8}$$

$$\nabla^2 \overrightarrow{A} = -\mu_0 \overrightarrow{j} \tag{9}$$

where V is the electric potential [V], $\overrightarrow{A}$ is the vector potential [N/A], and μ_0 is the permeability of free space [H/m].

In the model, generation of iron vapor from the tip of the electrode and the droplet is considered. The vapor distribution is described using the following equation:

$$\frac{\partial (\rho C)}{\partial t} + \nabla \cdot \left(\rho \overrightarrow{v} C \right) = -\nabla \cdot (-\rho D \nabla C) + S, \tag{10}$$

where C is the mass fraction of iron vapor, and D is the diffusion coefficient [m²/s] [19]. The iron vapor is generated according to the following equation:

$$J = \left(\frac{p_0}{\sqrt{T_{\text{Metal}}}} - \frac{p_{\text{Fe, vap}}}{\sqrt{T_{\text{Gas}}}} \right) \sqrt{\frac{M}{2\pi R}}, \tag{11}$$

where J is the mass flux of iron vapor [kg/m²/s], p_0 is the saturation vapor pressure of the iron vapor [Pa], $p_{\text{Fe, vap}}$ is the partial pressure of the iron vapor in the arc plasma [Pa], T_{Metal} is the temperature of the metal [K], T_{Gas} is the temperature of the arc plasma adjacent to the metal [K], M is the

0.38	0.09	0.00	Gaseous phase
1.00	0.79	0.15	0.00
Metal phase	1.00	0.99	0.88

$$\begin{cases} F = 0 & \text{in the gaseous phase} \\ 0 < F < 1 & \text{in the boundary region} \\ F = 1 & \text{in the metal phase} \end{cases}$$
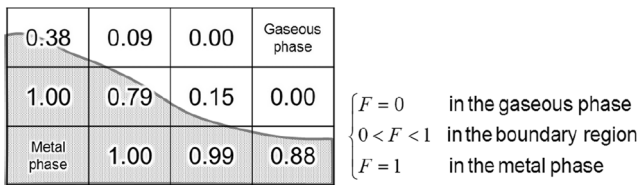
Fig. 2 Schematic image of VOF method

molecular weight of iron [kg/mol], and R is the ideal gas constant [J/mol/K]. The source terms S in Eqs. (1) and (10) and S_E in Eq. (3) were calculated using:

$$S = \nabla \cdot \overrightarrow{J}, \tag{12}$$

$$S_E = H_{\text{vap}} \nabla \cdot \overrightarrow{J}, \tag{13}$$

where H_{vap} is the heat of vaporization of iron [J/kg], $\overrightarrow{J} = -J\hat{n}$, and $\hat{n}$ is the unit normal vector calculated from the shape of the metal.

Next, the calculation method for the droplet is considered. The governing equations for the metal region were as follows:

$$\nabla \cdot \overrightarrow{v} = -\frac{1}{\rho} S, \tag{14}$$

$$\frac{\partial \overrightarrow{v}}{\partial t} + \nabla \cdot \left(\overrightarrow{v} \, \overrightarrow{v} \right) = -\frac{1}{\rho} \nabla P + \frac{1}{\rho} \nabla \cdot \overrightarrow{\tau} + \overrightarrow{g} + \overrightarrow{F}_{\text{ex}}, \tag{15}$$

$$\frac{\partial H}{\partial t} + \nabla \cdot \overrightarrow{v} H = -\frac{1}{\rho} \nabla \cdot (-\kappa \nabla T) + \frac{1}{\rho} W - \frac{1}{\rho} S_E, \tag{16}$$

where $\overrightarrow{F}_{\text{ex}}$ is the external force vector [N/m³], obtained by summing the electromagnetic force, the surface tension, the arc pressure, and the drag force due to the plasma flow.

The metal transfer and weld pool phenomena involve the deformation of a free surface, which was tracked in this model using the volume-of-fluid (VOF) method [20]. In the VOF method, the shape of a free surface is described by fluid occupancy using a so-called F value in each calculation cell, as shown in Fig. 2. According to the velocity field in the metal region, the free-surface deformation is calculated using the following equation:

$$\frac{\partial F}{\partial t} + \left(\overrightarrow{v} \cdot \nabla \right) F = 0. \tag{17}$$

The surface tension force was calculated using the continuum surface force (CSF) model [21], in which the capillary pressure of the surface tension acting on the liquid phase is expressed as a volume force in the surface region. This can be calculated as follows:

$$\overrightarrow{F}_{\text{ST}} = \gamma \kappa_{\text{curv}} \, \overrightarrow{n}, \tag{18}$$

where $\overrightarrow{F}_{\text{ST}}$ is the equivalent volume force vector of the capillary pressure of the surface tension [N/m³], γ is the surface tension [N/m], κ_{curv} is the curvature [1/m], and $\overrightarrow{n}$ is the normal vector [1/m].

In this model, sheath regions formed near the wire electrode and the base metal are not resolved. Their influence is taken into account though additional energy fluxes at the surface of the wire electrode, which is the anode, and the base metal, which is the cathode. These energy fluxes are given by the following equations: *Wire electrode (anode)*:

$$\overrightarrow{q}_{\text{Anode}} = -\overrightarrow{j} \, \varphi_{\text{Anode}} - \varepsilon \alpha T_{\text{Metal}}^4 \hat{n}, \tag{19}$$

Base metal (cathode):

$$\overrightarrow{q}_{\text{Cathode}} = -\overrightarrow{j}_e \varphi_{\text{Cathode}} + \overrightarrow{j}_i V_i - \varepsilon \alpha T_{\text{Metal}}^4 \hat{n}, \tag{20}$$

where $\overrightarrow{q}_{\text{Anode}}$ and $\overrightarrow{q}_{\text{Cathode}}$ are respectively the energy fluxes at the anode and cathode surfaces [W/m²], φ_{Anode} and φ_{Cathode} are respectively the work functions of the

Fig. 3 Schematic image and boundary conditions for the model
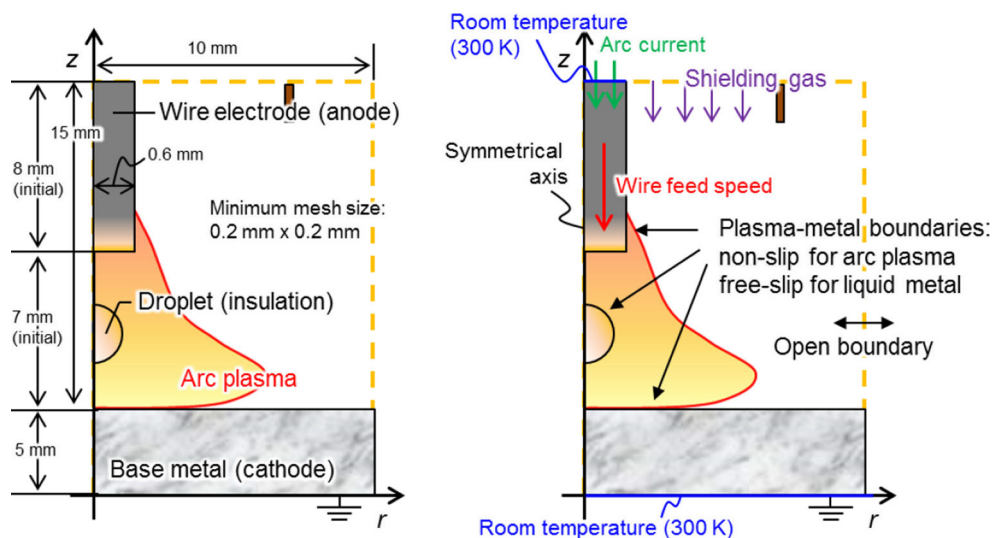
Table 1 Physical properties of mild steel

Density [kg/m^3]	7200
Viscosity [Pas]	6×10^{-3}
Thermal conductivity [W/mK]	26–52
Specific heat [J/kgK]	695–800
Electrical conductivity [S/m]	7.7×10^5
Surface tension [N/m]	1.2
Work function [V]	4.3
Melting temperature [K]	1750
Latent heat of fusion [J/kg]	2.47×10^5
Boiling temperature [K]	3080
Latent heat of vaporization [J/kg]	7.34×10^6
Radiation emissivity	0.4

anode and cathode [V], $\overrightarrow{j}_i$ and $\overrightarrow{j}_e$ are respectively the ion and electron current densities [A/m^2], ε is the radiative emissivity, and α is the Stefan–Boltzmann constant [W/m^2/K^4]. These governing equations are solved in two-dimensional axially symmetric geometry by our computer code. The velocity and pressure fields of the arc plasma and the molten metal are calculated using the simplified marker and cell (SMAC) method [22]. A schematic image and the boundary conditions for the model are shown in Fig. 3. The welding torch and base metal are assumed to be stationary. The wire electrode and the base metal are mild steel, and the material properties used for the metal are shown in Table 1 [23, 24]. The diameter of the wire electrode is 1.2 mm, the distance between the contact tip and the base metal is 15 mm, and the time step is 1×10^{-4} s. Pure argon and an Ar + 18 %CO$_2$ mixture are used in order to investigate the influence of the shielding gas. However, the material properties of the plasma gas are changed remarkably by the influence of iron vapor. The material properties of the plasma gas, including the influence of iron vapor, were taken from the work of Murphy [25]. The temperature dependence of the thermal conductivity and the specific heat without the iron vapor are shown in Fig. 4.
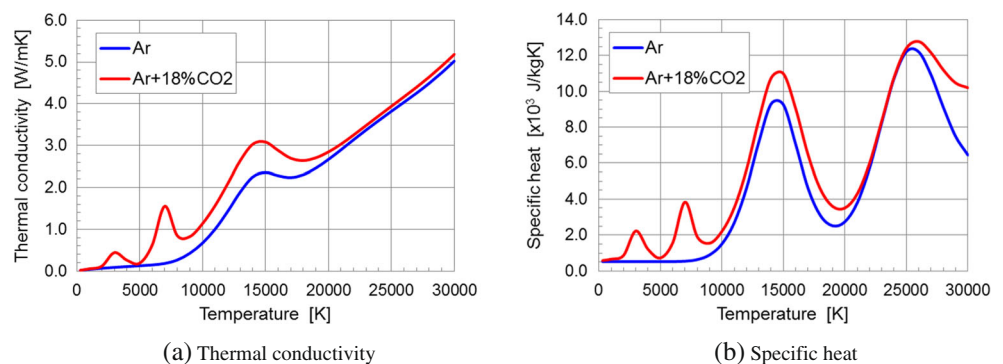
3 Results and discussion

3.1 Setting the initial conditions

The initial conditions for the calculations are first shown. The initial conditions for the metal region are shown in Fig. 5a. The base metal is set to room temperature (300 K). The temperature of the wire electrode is set to room temperature at the contact tip and the melting temperature at the bottom tip. In addition, the initial droplet is attached to the bottom tip of the wire electrode. The initial droplet is hemispherical in shape, and its temperature is 2500 K. The initial condition for the arc plasma is that calculated for steady state with the initial condition of the metal region. Figure 5b, c shows the initial conditions for the arc plasma using pure argon and the gas mixture, respectively. The arc current is 260 A. When the gas mixture is used, the maximum temperature increases, and the shape of the arc plasma becomes constricted. This is because the specific heat of the Ar–CO$_2$ mixture is higher than that of pure argon as was shown in Fig. 4 [26].

3.2 Setting the wire feeding speed

It is necessary to set the appropriate wire feeding speed because wire melting is included in the model. The appropriate wire feeding speed should be equal to the wire melting speed in order to maintain a constant arc length. The wire melting speed depends on the arc current. In this study, the wire feeding speed that maintains the length of the solid region of the wire electrode at 8 mm (the initial condition) is employed as the appropriate value. The appropriate wire feeding speed obtained by our model is shown in Fig. 6; it is independent of the shielding gas.

3.3 Influence of the arc current on the metal transfer

The results obtained for time-dependent calculations of the arc plasma and molten metal are now presented. Figure 7

Fig. 4 Thermal properties of the two shielding gases: **a** Thermal conductivity and **b** specific heat

(a) Thermal conductivity

(b) Specific heat

Fig. 5 Initial conditions for calculations (arc current: 260 A): **a** metal temperature, **b** temperature of Ar gas, **c** temperature of gas mixture

(a) Metal temperature   (b) Temperature of Ar gas   (c) Temperature of gas mixture
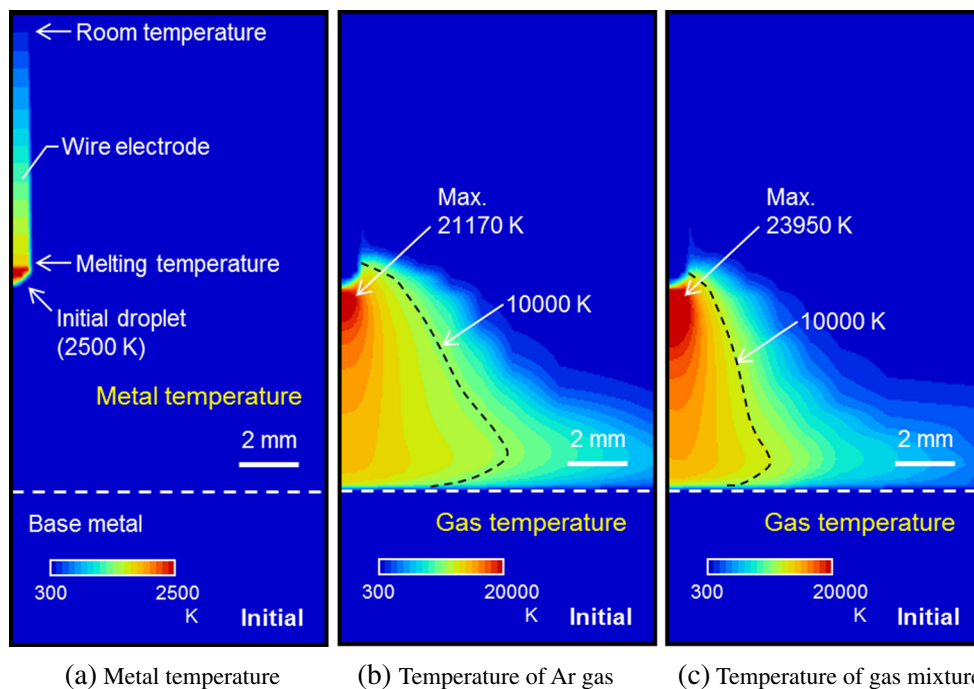
shows the results obtained using pure argon and Ar–CO$_2$ mixture when the arc current is set to 260 A. The left-hand sides of the figures show the metal temperature, and the right-hand sides show the gas temperature. Figure 7a shows the calculation results using pure argon. The droplets detaching from the wire tip are small, and the metal transfer mode can be regarded as spray transfer. On the other hand, when the gas mixture is used, the droplet becomes large, and the transfer mode can be regarded as globular transfer, as shown in Fig. 7b. The results indicated that even if the arc currents are set to be the same, the transfer mode differs, depending on the shielding gas. The mechanism that causes this difference is discussed in Section 3.4. The temperature of the arc plasma reaches a relatively low value as the droplet grows. Just after the droplet detaches from the wire tip, the arc temperature increases. The maximum temperature of the droplets is

around 3000 K when the droplet is attached to the wire tip, decreasing to around 2900 K after the droplet detaches from the wire tip.

Figure 8 shows the relationship between the arc current and the transfer frequency of the droplet. When pure argon is used, the frequency significantly increases as the current is increased to around 230 A. This means that the transfer mode changes from globular to spray transfer at this current. We call this current the "transition current." On the other hand, in the case where the gas mixture is used, the transfer frequency increases at around 280 A. The transition current for the mixed-gas arc is higher than that for the argon arc.

Figure 9 shows the relationship between the arc current and the average droplet temperature. Compared with Fig. 8, the average droplet temperature in globular transfer is around 2700 K, and in spray transfer, it is around 2900 K. Since the droplet volume significantly changes, depending on the transfer mode, the average droplet temperature also depends on the transfer mode.
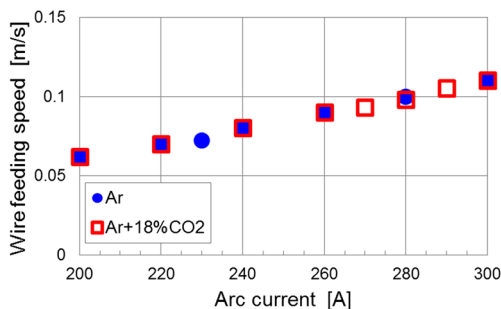
3.4 Discussion

In this section, the mechanism by which the transfer mode depends on the shielding gas is discussed. The arc pressure acting on the droplet is presumed to be an important factor. It acts to lift up the droplet, and if it becomes stronger, it interferes with the detachment of the droplet from the wire tip. Figure 10 shows the time evolution of the average pressure acting on the droplet. When pure argon is used,

Fig. 6 Relationship between arc current and wire feeding speed in the model
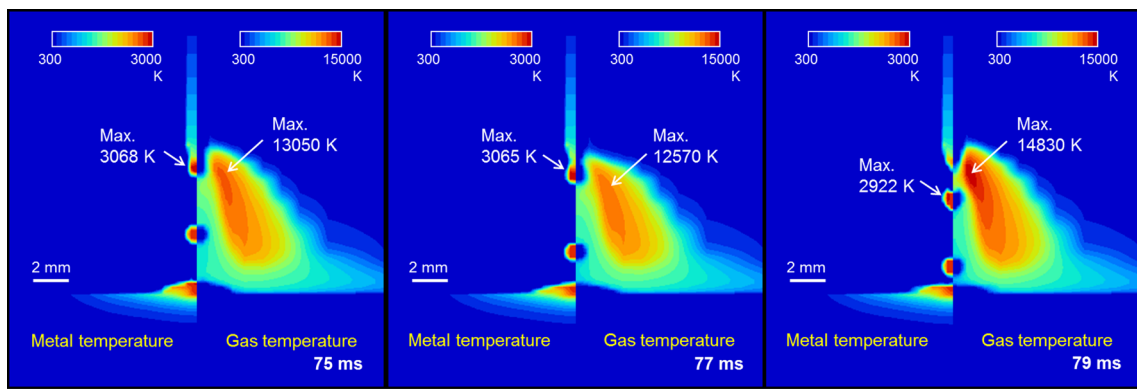
(a) Ar
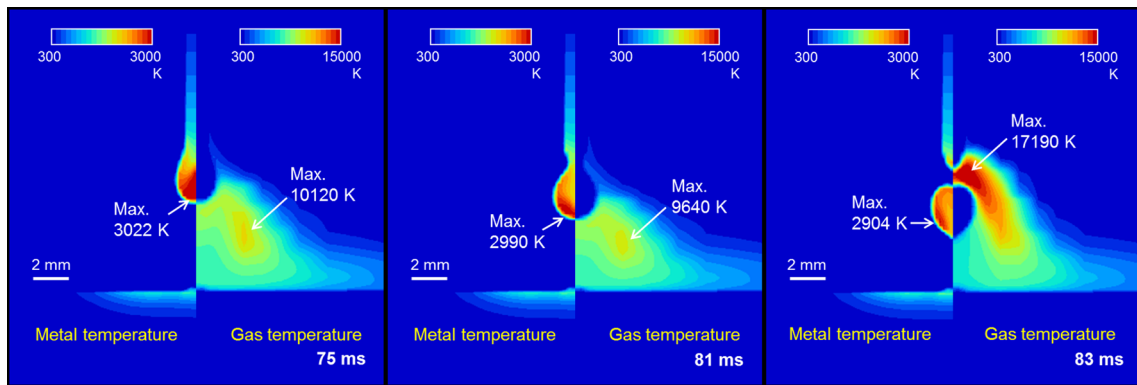
(b) Ar+18%CO$_2$

Fig. 7 Influence of shielding gas on gas and metal temperature (arc current: 260 A): **a** Ar, **b** Ar + 18%CO2

the average pressure is around 500 Pa, and it changes very little with time. In the case of the gas mixture, the average pressure changes significantly with time. The shape of the droplets is also shown in the figure; when the average pressure of the arc in the gas mixture rises, the droplet is in the early phase of its growth. The surface area of the droplet increases as the droplet grows, and the average pressure decreases.

This difference in arc pressure is caused by the difference in the current path in the arc plasma. Figure 11 shows

the electrical conductivity and the current density distribution near the wire tip at the early phase of droplet growth. When the gas mixture is used, the maximum current density is higher. Moreover, when pure argon is used, the maximum current density occurs at the side of the forming droplet. On the other hand, for the gas mixture, the current density is concentrated at the bottom of the forming droplet.

Figure 12 shows the temperature and iron vapor concentration distributions in the arc plasma. When pure
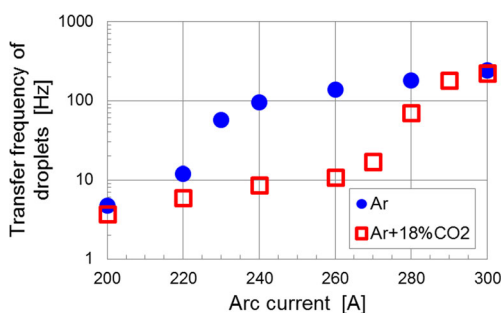

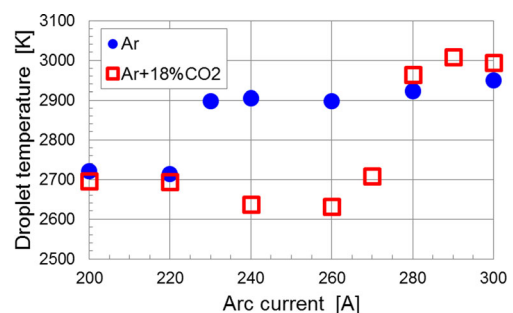**Fig. 8** Influence of arc current on transfer frequency of droplets

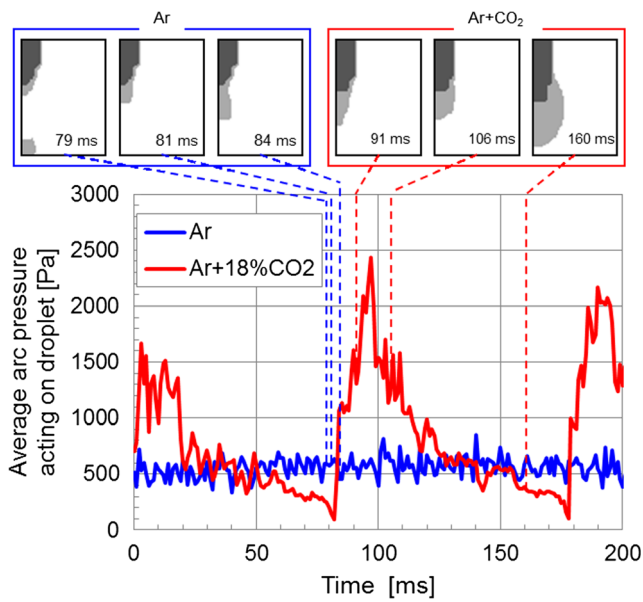**Fig. 9** Influence of arc current on average droplet temperature

Fig. 10 Change in average arc pressure acting on droplet over time

argon is used, the temperature of the central region of the arc plasma is low due to the large concentration of iron vapor, and 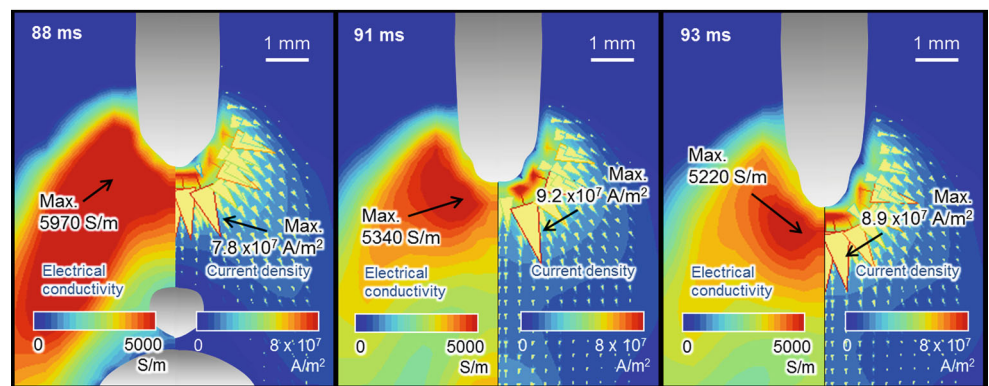a high-temperature region is formed at the side of the forming droplet, which is outside the region of high iron-vapor concentration. For this reason, a current path forms at the side of the forming droplet, as shown in Fig. 11. On the other hand, when the gas mixture is used, the arc plasma temperature is low not just in the central region but all around the forming droplet. In this case, a relatively high-temperature region forms at the bottom of the forming droplet, which is inside the region of high iron-vapor concentration. For this reason, the difference in the electrical conductivity of the arc plasma between the side of the forming droplet and the bottom of the forming droplet is small. Once this electrical conductivity distribution has developed, the current density becomes concentrated on the bottom tip of the forming droplet, which is the closest point to the base metal. Consequently, when the gas mixture is used, a high-temperature region is formed in the region of high iron-vapor concentration.

Concluding these discussions, when the gas mixture is used, the temperature of the arc plasma becomes low over a wide area surrounding the forming droplet due to the influence of the iron vapor generated from the droplet in the early stages of droplet growth. For this reason, the difference in the electrical conductivity of the arc plasma

Fig. 11 Electrical conductivity and current density distributions near wire electrode: **a** Ar, **b** Ar + 18%CO2
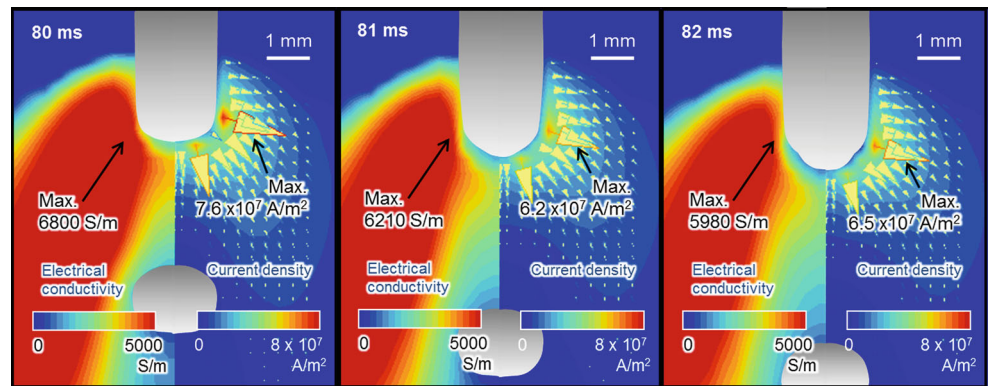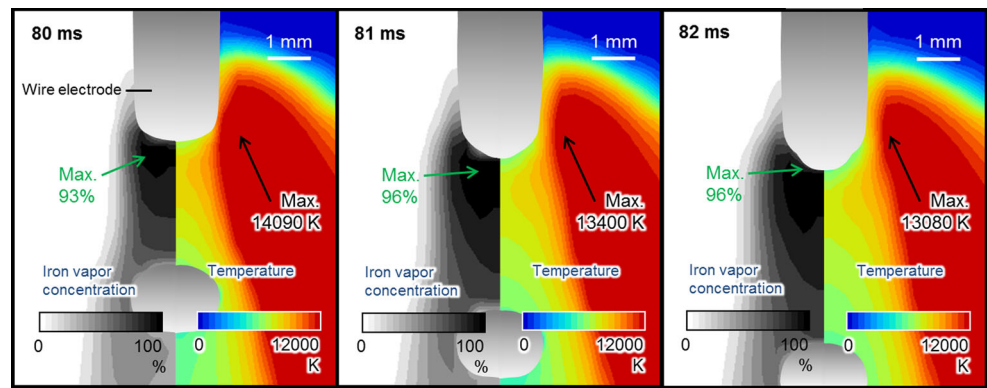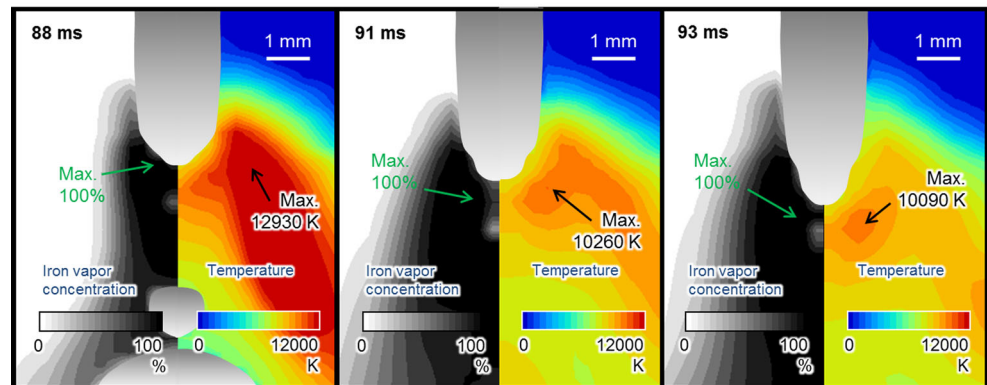
(a) Ar

(b) Ar+18%CO_2

Fig. 12 Temperature and iron vapor distributions near the wire electrode: **a** Ar, **b** Ar + 18%CO2

(a) Ar

(b) Ar+18%CO$_2$

between the side and the bottom of the droplet becomes small, and a region of high-temperature is formed in the center of the arc plasma near the droplet. Consequently, the current density becomes concentrated at the bottom of the droplet, and the arc pressure becomes high. This arc pressure lifts up the droplet and prevents detachment from the wire tip. Therefore, in the case of the gas mixture, it is difficult for the spray transfer mode to occur, and the transition current become higher than that for pure argon.

This difference of the property of the droplet transfer is caused by differences between the material properties of pure argon and that of the gas mixture. In this study, the difference of their specific heat, as shown in Fig. 4b, is important. When the gas mixture is used, the shape of arc plasma becomes constricted because of its larger specific heat. When the metal vapor generates from the electrode tip in the early stages of droplet growth, if the pure argon is used, since the shape of arc plasma is relatively large, a high-temperature region at the side of droplet remains and the current path is easily formed at the side of the arc plasma. On the other hand, if the gas mixture is used, because of its constricted shape, a high-temperature region cannot be formed at the side of

the droplet and the current path is formed at the center of arc plasma.

4 Conclusion

In this study, the influence of the shielding gas on the metal transfer phenomena was numerically investigated. The results obtained are summarized as follows:

(1) When pure argon is used, the current at which the metal transfer changes from globular to spray mode is around 230 A. In the case of mixed gas, the transition current is around 280 A.

(2) The average droplet temperature depends on the transfer mode. The temperature is around 2700 K for globular transfer and around 2900 K for spray transfer.

(3) When the Ar–CO$_2$ mixture is used, the arc plasma becomes constricted in shape because of its larger specific heat. In the early stages of droplet growth, the current density is concentrated at the bottom tip of the droplet. Consequently, the arc pressure that lifts up the droplet becomes stronger. For this reason, the transition current is higher for the gas mixture.

References

1. Ruckdeschel WEW (1976) Classification of metal transfer, IIW Doc. XII-636-76
2. Ludwig HC (1957) Metal transfer characteristics in gas-shielded arc welding. Weld J 36:23s–26s
3. Needham JC, Cooksey CJ, Milner DR (1960) Metal transfer in inert-gas shielded-arc welding. Br Weld J 7:101–114
4. Liu S, Siewert TA (1989) Metal transfer in gas metal arc welding: droplet rate. Weld J 68:52s–58s
5. Lesnewich A (1958) Control of melting rate and metal transfer in gas-shielded metal-arc welding part II—control of metal transfer. Weld J 37:418s–425s
6. Rhee S, Kannatey-Asibu E Jr (1992) Observation of metal transfer during gas metal arc welding. Weld J 71:381s–386s
7. Simpson SW, Zhu P (1995) Formation of molten droplet at a consumable anode in an electric welding arc. J Phys D Appl Phys 28: 1594–1600
8. Choi SK, Yoo CD, Kim Y-S (1998) Dynamic simulation of metal transfer in GMAW, part 1: globular and spray transfer modes. Weld J 77:38s–44s
9. Choi SK, Yoo CD, Kim Y-S (1998) The dynamic analysis of metal transfer in pulsed current gas metal arc welding. J Phys D Appl Phys 31:207–215
10. Wang G, Huang PG, Zhang YM (2003) Numerical analysis of metal transfer in gas metal arc welding. Metall Mater Trans B 34B:345–353
11. Kadota K, Hirata Y (2011) Numerical model of metal transfer using an electrically conductive liquid. Weld World 55(09/10):50–55
12. Wang F, Hou WK, Hu SJ, Kannatey-Asibu E, Schultz WW, Wang PC (2003) Modelling and analysis of metal transfer in gas metal arc welding. J Phys D Appl Phys 36:1143–1152
13. Haidar J, Lowke JJ (1996) Predictions of metal droplet formation in arc welding. J Phys D Appl Phys 29:2951–2960
14. Hu J, Tsai HL (2007) Heat and mass transfer in gas metal arc welding. Part II: the metal. Int J Heat Mass Transf 50:808–820
15. Xu G, Hu J, Tsai HL (2009) Three-dimensional modeling of arc plasma and metal transfer in gas metal arc welding. Int J Heat Mass Transf 52:1709–1724
16. Hertel M, Spille-Kohoff A, Fuessel U, Schnick M (2013) Numerical simulation of droplet detachment in pulsed gas-metal arc welding including the influence of metal vapour. J Phys D Appl Phys 46:224003
17. Ogino Y, Hirata Y (2015) Numerical simulation of metal transfer in argon gas-shielded GMAW. Weld World 59:465–473
18. Haidar J, Lowke JJ (1997) Effect of CO2 shielding gas on metal droplet formation in arc welding. IEEE Trans Plasma Sci 25(5): 931–936
19. Wilke CR (1950) A viscosity equation for gas mixtures. J Chem Phys 18(4):517–519
20. Hirt CW, Nichols BD (1981) Volume of Fluid (VOF) method for the dynamics of free boundaries. J Comput Phys 39: 201–225
21. Brackbill JU, Kothe DB, Zamach C (1992) A continuum method for modeling surface tension. J Comput Phys 100:335–354
22. Amsden AA, Harlow FH (1970) The SMAC method: a numerical technique for calculating incompressible fluid flows. Los Alamos Science Laboratory Report, LA-4370
23. Rao ZH, Hu J, Liao SM, Tsai HL (2010) Modeling of the transport phenomena in GMAW using argon–helium mixtures. Part I—the arc. Int J Heat Mass Transf 53:5707–5721
24. Ushio M, Wu CS (1997) Mathematical modeling of three-dimensional heat and fluid flow in a moving gas metal arc weld pool. Metall Mater Trans B 28B:509–516
25. Murphy AB (2010) The effects of metal vapour in arc welding. J Phys D Appl Phys 43:434001
26. Tanaka M, Lowke JJ (2007) Predictions of weld pool profiles using plasma physics. J Phys D Appl Phys 40:R1–R23